ISSN 0023-1584, Kinetics and Catalysis, 2006, Vol. 47, No. 6, pp. 812–824. © MAIK "Nauka/Interperiodica" (Russia), 2006.
Original Russian Text © A.N. Ermakov, I.K. Larin, A.A. Ugarov, A.P. Purmal, 2006, published in Kinetika i Kataliz, 2006, Vol. 47, No. 6, pp. 836–848.

Drop Size Effect on the Rate and Mechanism of SO_2 Oxidation in Tropospheric Clouds

A. N. Ermakov[a], I. K. Larin[a], A. A. Ugarov[a], and A. P. Purmal[b]

[a] *Institute of Energy Problems of Chemical Physics, Russian Academy of Sciences, Chernogolovka, Moscow oblast, 142432 Russia*

[b] *Semenov Institute of Chemical Physics, Russian Academy of Sciences, Moscow, 117977 Russia*

e-mail: ayermakov@chph.ras.ru

Received July 5, 2005

Abstract—The drop size effect on the rate and mechanism of sulfur dioxide oxidation in tropospheric clouds is analyzed. In the daytime, the oxidation rate decreases as the drops grow. This effect is due to the fact that the liquid-phase reactions slow down because of a decreasing influx of oxidizing species, namely, H_2O_2, $OH^{\bullet}$, $HO_2^{\bullet}$, and O_3. The effect of the nonuniformity of $OH^{\bullet}$ and O_3 distribution in the drop bulk on the reaction rate is discovered.

DOI: 10.1134/S0023158406060024

Hydrophilic substances, including $SO_{2(g)}$ and $NO_{2(g)}$ [1], are absorbed from the air by cloud droplets to be oxidized there. It has been established by field (Great Dun Fell, GDF) experiments that most of the atmospheric $SO_{2(g)}$ is oxidized just in cloud droplets [2].[1] In the daytime, this self-cleaning is due to $O_{3(g)}$, $H_2O_{2(g)}$, and $O_{2(g)}$ influx from the gas phase [3]. The oxidation with oxygen involves the $SO_{3-5(aq)}^{-\bullet}$ radical [4]. The formation of this radical is an indirect result of the entrainment of $OH_g^{\bullet}$ and, to a lesser extent, $NO_{3(g)}^{\bullet}$ from the gas phase [5] and of the liquid-phase photolysis of $H_2O_{2(aq)}$, $NO_{3(aq)}^{-}$ [1], $FeOH_{(aq)}^{2+}$ [6], etc. The extent of $OH_g^{\bullet}$ entrainment is illustrated, e.g., by the 2- to 3-fold decrease in the hydroxyl concentration recently observed in a cloud zone [7]. No matter what the mechanism of the liquid-phase processes in clouds, the dynamics of these processes is governed by the liquid-water content of the gas ($L = V_{aq}/V_g$, where V is the volume of the phase) and by the drop radius (r_0). The origination of size effects in atmospheric chemical reactions [8] can readily be understood by analyzing the effect of drop growth at a constant L.

An increasing drop size not only causes an obvious deceleration of the liquid-phase reactions because of a decreasing flux of $OH_g^{\bullet}$ and other radicals but also slows down the liquid-phase transport of entrained species: $\tau_{aq} = r_0^2/\pi^2 D_{aq}(i)$ [9], where τ_{aq} is the characteristic time of diffusion in the drop and $D_{aq}(i)$ is the diffusion coefficient. The characteristic time of transport increases with increasing r_0, and, in large drops, it can exceed the characteristic time of the chemical reaction. The competition between these processes is also influenced by the reactivity of the species entrained from the gas. The higher the reactivity of the species, the smaller the drop size at which the diffusion limitations come into play. The entrainment of species from the gas phase is accompanied by reactions occurring in the subsurface layer of the drop, which result in a nonuniform distribution of entrained species in the drop volume. Under these conditions, most of the impinging species return to the gas phase [8]. However, the growth of drops may be accompanied by the opposite process, which is favored by chemical and photochemical reactions generating free radicals in the bulk of the drop [8]. The net effect of the near-surface and bulk reactions involving free radicals on the rates of the oxidation reactions in the water droplets of tropospheric clouds has not been studied adequately [8, 10, 11]. Here, we consider this effect in the oxidation of atmospheric $SO_{2(g)}$, which is the main source of acidic precipitation.

Box Model of the Convective Cloud

Our kinetic analysis of chemical processes in clouds will be based on the reduced model (RM) of atmospheric $SO_{2(g)}$ oxidation [12]. In this work, RM is used in the simulation of the self-cleaning dynamics of air heavily polluted with sulfur dioxide (Table 1). Events

[1] The studies quoted here are part of the field investigation of atmospheric phenomena carried out in the framework of a EUROTRAC project (subproject Ground-Based Cloud Experiment).

Table 1. Gas composition and the initial concentrations of gas components in the reduced model (RM)

Component	Concentration, cm^{-3}	Component	Concentration, cm^{-3}	Component	Concentration, cm^{-3}	Component	Concentration, cm^{-3}
CH_2O_g	2.55×10^9	CO_g	3.62×10^{12}	$HNO_{2(g)}$	6.10×10^6	$NO_{2(g)}$	6.40×10^8
$CH_2OH_g^{\cdot}$	1.23×10^3	$CO_{2(g)}$	8.40×10^{15}	$HNO_{3(g)}$	4.00×10^9	$NO_{3(g)}$	7.00×10^4
$CH_{3(g)}^{\cdot}$	5.19×10^{-3}	H_g	5.43×10^{-2}	$HNO_{4(g)}$	6.60×10^6	O_g	2.48×10^3
$CH_3O_g^{\cdot}$	3.77×10^1	$H_{2(g)}$	2.55×10^{13}	$HO_{2(g)}^{\cdot}$	6.00×10^8	$O(^1D)_g$	1.28×10^{-3}
$CH_3O_{2(g)}^{\cdot}$	4.56×10^8	H_2O_g	5.94×10^{17}	$N_{2(g)}$	1.92×10^{19}	$O_{2(g)}$	5.34×10^{18}
CH_3OH_g	4.44×10^{10}	$H_2O_{2(g)}$	2.55×10^{10}	N_2O_g	7.65×10^{12}	$O_{3(g)}$	8.01×10^{11}
$CH_{4(g)}$	4.15×10^{13}	$HCO_g^{\cdot}$	7.31×10^{-3}	$N_2O_{5(g)}$	7.13×10^2	$OH_g^{\cdot}$	4.00×10^6
$CH_4O_{2(g)}^{\cdot}$	7.46×10^{10}			NO_g	2.60×10^8	$SO_{2(g)}$	9.00×10^{10}

of the self-cleaning of a continental atmosphere with a similar $SO_{2(g)}$ content have been observed, e.g., in GDF experiments [2]. Our research has so far been limited to the role of small drops (r_0 = 1 μm) in air self-cleaning [12]. Here, we focus on the drop size effect in this process.

The size and volumetric concentration of drops in tropospheric clouds vary widely. Averaging these parameters over a large number cloud generation events and various cloud types leads to the following inferences. The size of most of the drops is between a few and ~10 μm. The drop concentration ranges between tens and ~10^3 cm^{-3}. The concentration of large drops with a radius above 10^2 μm is usually lower by a factor of 10^3–10^5. During rainfall, this concentration increases, which is evidence of the variability of the size distribution of cloud drops [13]. According to earlier reports [14–16], large drops are present not only in rain clouds but also in ordinary clouds. It is essential that, in spite of their low concentration, they may contain a considerable amount of liquid water. For example, for drops with r_0 = 5 μm, whose concentration in the cloud is the highest, the corresponding normalized amount of liquid water (L/r_0) is 3×10^{-8} μm^{-1} [17]; that is, $L \approx 1.5 \times 10^{-7}$. For raindrops with $r_0 = 10^3$ μm, which precipitate with a velocity of 10 mm/h, the normalized amount of liquid is 3×10^{-10} μm^{-1} [18] and, hence, $L \approx 3 \times 10^{-7}$. The variation of the dynamics of chemical processes during the lifetime of a cloud was beyond the scope of our analysis. All calculations were carried out under the assumption that the liquid water occupies a constant fraction of the gas volume ($L = 10^{-6}$).

The drop size effect on the dynamics of chemical and photochemical processes in the atmosphere has been the subject of a number of publications. Here, we use a mathematical approach suggested by Schwartz and Freiberg [9]. The essence of this approach is briefly described below.[2] In an earlier study, this approach was

[2] According to Schwartz and Freiberg [9], the steady-state distribution of a model reagent in drops is analyzed in terms of the equation

$$D_{aq}\frac{1}{r^2}\frac{d}{dr}\left(r^2\frac{dC_{aq}}{dr}\right) - k_L(r)C_{aq} + P(r) = 0$$

subject to the boundary conditions $(dC_{aq}/dr)_{r=0} = 0$ and $C_{aq}(r_0) = C_{aq}^*$. Here, C_{aq} is the reactant concentration in the liquid at the distance r from the drop center, $k_L(r)$ is the effective first-order rate constant of reactant consumption (s^{-1}), and C_{aq}^* is the reactant concentration on the drop surface. The consumption of the reactant in second-order reactions is neglected because of the low rates of these reactions [9]. The term $P(r)$ in the above equation is the rate of generation of the reactant by liquid-phase chemical and photochemical reactions. The solution of this equation for $P(r) = 0$ is presented in [9]. It has been demonstrated that C_{aq}^* can be calculated using the drop-average reactant concentration $\bar{C}_{aq}$:

$$C_{aq}^* = \bar{C}_{aq}\left[3\left(\frac{\coth(q)}{q} - \frac{1}{q^2}\right)\right]^{-1}.$$

Here, $\coth(q)$ is the hyperbolic cotangent and $q = r_0\xi_i$ is a dimensionless parameter, where $\xi_i = (k_{L(i)}/D_{aq})^{1/2}$ (cm^{-1}) is a quantity characterizing the so-called reaction length of the reagent (l_i). Some complication arises for $P(r) \neq 0$. Even in this case, it is still possible to relate C_{aq}^* to $\bar{C}_{aq}$ [8].

Table 2. Chemical reactions in water drops

No.	Reaction	k_{iA}, $l\ mol^{-1}\ s^{-1}$	No.	Reaction	k_{iA}, $l\ mol^{-1}\ s^{-1}$
1A	$HO^{\bullet}_{2(aq)} + HO^{\bullet}_{2(aq)} \longrightarrow H_2O_{2(aq)} + O_{2(aq)}$	8.3×10^5	13A	$SO^{2-}_{3(aq)} + O_{3(aq)} \longrightarrow SO^{2-}_{4(aq)} + O_{2(aq)}$	1.5×10^9
2A	$HO^{\bullet}_{2(aq)} + O^{-\bullet}_{2(aq)} \xrightarrow{H_2O} H_2O_{2(aq)} + O_{2(aq)} + OH^{-}_{aq}$	9.7×10^7	14A	$HSO^{-}_{3(aq)} + O_{3(aq)} \longrightarrow HSO^{-}_{4(aq)} + O_{2(aq)}$	3.7×10^5
3A*	$HSO^{-}_{3(aq)} + H_2O_{2(aq)} + H^{+}_{aq} \longrightarrow SO^{2-}_{4(aq)} + H_2O + 2H^{+}_{aq}$	6.9×10^7	15A	$SO^{-\bullet}_{4(aq)} + HSO^{-}_{3(aq)} \longrightarrow HSO^{-}_{4(aq)} + SO^{-\bullet}_{3(aq)}$	3.2×10^8
4A	$SO^{2-}_{3(aq)} + OH^{\bullet}_{aq} \longrightarrow OH^{-}_{aq} + SO^{-\bullet}_{3(aq)}$	4.6×10^9	16A	$SO^{-\bullet}_{4(aq)} + SO^{2-}_{3(aq)} \longrightarrow SO^{2-}_{4(aq)} + SO^{-\bullet}_{3(aq)}$	3.2×10^8
5A	$HSO^{-}_{3(aq)} + OH^{\bullet}_{aq} \longrightarrow H_2O + SO^{-\bullet}_{3(aq)}$	2.7×10^9	17A	$SO^{-\bullet}_{5(aq)} + HO^{\bullet}_{2(aq)} \longrightarrow HSO^{-}_{5(aq)} + O_{2(aq)}$	1.7×10^9
6A*	$HSO^{-}_{5(aq)} + HSO^{-}_{3(aq)} + H^{+}_{aq} \longrightarrow 2SO^{2-}_{4(aq)} + 3H^{+}_{aq}$	1.0×10^7	18A	$SO^{-\bullet}_{5(aq)} + O^{-\bullet}_{2(aq)} \longrightarrow SO^{2-}_{5(aq)} + O_{2(aq)}$	1.7×10^9
7A	$N_2O_{5(aq)} + H_2O \longrightarrow 2H^{+}_{aq} + 2NO^{-}_{3(aq)}$	5.0×10^9	19A	$SO^{-\bullet}_{5(aq)} + HSO^{-}_{3(aq)} \longrightarrow SO^{2-}_{4(aq)} + SO^{-\bullet}_{4(aq)} + H^{+}_{aq}$	2.0×10^2
8A	$NO^{\bullet}_{3(aq)} + HSO^{-}_{3(aq)} \longrightarrow NO^{-}_{3(aq)} + SO^{-\bullet}_{3(aq)} + H^{+}_{(aq)}$	1.3×10^9	20A	$SO^{-\bullet}_{5(aq)} + HSO^{-}_{3(aq)} \longrightarrow HSO^{-}_{5(aq)} + SO^{-\bullet}_{3(aq)}$	3.4×10^3
9A	$NO^{\bullet}_{3(aq)} + SO^{2-}_{3(aq)} \longrightarrow NO^{-}_{3(aq)} + SO^{-\bullet}_{3(aq)}$	3.0×10^8	21A	$SO^{-\bullet}_{5(aq)} + SO^{2-}_{3(aq)} \longrightarrow SO^{-\bullet}_{4(aq)} + SO^{2-}_{4(aq)}$	5.5×10^5
10A	$O^{-\bullet}_{2(aq)} + O_{3(aq)} \xrightarrow{H^{+}} 2O_{2(aq)} + OH^{\bullet}_{aq}$	1.5×10^9	22A	$SO^{-\bullet}_{5(aq)} + SO^{2-}_{3(aq)} \longrightarrow SO^{2-}_{5(aq)} + SO^{-\bullet}_{3(aq)}$	2.1×10^5
11A	$SO_2 + O_3 \xrightarrow{H_2O} HSO^{-}_{4(aq)} + O_{2(aq)} + H^{+}_{aq}$	2.4×10^4	23A	$SO^{-\bullet}_{5(aq)} + SO^{-\bullet}_{5(aq)} \longrightarrow S_2O^{2-}_{8(aq)} + O_{2(aq)}$	1.3×10^7
12A	$SO^{-\bullet}_{3(aq)} + O_{2(aq)} \longrightarrow SO^{-\bullet}_{5(aq)}$	2.5×10^9	24A	$SO^{-\bullet}_{5(aq)} + SO^{-\bullet}_{5(aq)} \longrightarrow 2SO^{-\bullet}_{4(aq)} + O_{2(aq)}$	8.7×10^7

* The rate constant of this reaction has dimensions of $l^2\ mol^{-2}\ s^{-1}$.

used in the simulation of sulfur dioxide and formaldehyde oxidation in the marine atmosphere.[3]

The set of differential equations was numerically integrated for a unit volume of a gas uniformly filled with monodisperse drops, taking into account earlier reports [8, 9]. In the framework of RM, concentration averaging as in [8, 9] was made for $OH^{\cdot}_{aq}$, $O_{3(aq)}$, and $NO^{\cdot}_{3(aq)}$.[4] The drop size was varied between 0.1 and 10^3 μm [17–19]. All calculations for the dynamics of liquid-phase processes were carried out under the assumption that, even in the largest drops, the transport of reactants is only due to molecular diffusion [20]. The calculated data presented below refer to the daytime. The photodissociation coefficients of the light-sensitive components of the gas phase were calculated for the noontime of the day of equinox at 60° N and a height of 1 km [12]. The photodissociation coefficient data for liquid-phase components were taken from [1, 10]. The scattering of UV radiation on the surface and in the bulk of a convective cloud was neglected. The integration time (t_{exp}) was varied between 0 and 10^4 s. The chemical and photochemical processes in the gas and liquid phases, as well as their kinetic and thermodynamic parameters, were taken to be the same as in our earlier work [12]. For this reason, here we present only the liquid-phase data necessary for discussion (Tables 2–4).

Table 3. Photodissociation processes in the liquid phase

No.	Process	J_{lA}, s^{-1}
36A	$NO^-_{2(aq)} \xrightarrow[h\nu]{H_2O} NO_{aq} + OH^{\cdot}_{aq} + OH^-_{aq}$	2.6×10^{-5}
37A	$H_2O_{2(aq)} \xrightarrow{h\nu} 2OH^{\cdot}_{aq}$	7.2×10^{-6}
38A	$NO^-_{3(aq)} \xrightarrow[h\nu]{H_2O} NO_{2(aq)} + OH^{\cdot}_{aq} + OH^-_{aq}$	4.3×10^{-7}

Note: J_{iA} is the photodissociation coefficient of the component in the liquid-phase.

$OH^{\cdot}_{aq}$ Radical

Figure 1 plots the calculated drop-average concentration of hydroxyl radicals ($\overline{[OH^{\cdot}_{aq}]}$) as a function of r_0 for two different t_{exp} values. In these calculations, we took into account both the variation of the radical flux (hereafter referred to as the *S*/*V* factor for brevity) and the nonuniformity of $OH^{\cdot}_{aq}$ and ozone distribution in the drop bulk. Clearly, the $OH^{\cdot}_{aq}$ concentration varies nonmonotonically as the drop grows. For small drops (0.1–1 μm), $\overline{[OH^{\cdot}_{aq}]}$ is nearly constant. This constancy of $\overline{[OH^{\cdot}_{aq}]}$ persists in spite of the fact that the interfacial area and the volumetric concentration of drops decrease by a factor of 10 and 10^3, respectively. The descending portions of the $\overline{[OH^{\cdot}_{aq}]}$ curves indicate that, as the drop grows from 1 to 1000 μm, the concentration of hydroxyl radicals decreases less rapidly than the $OH^{\cdot}_{g}$ flux from the gas (the $OH^{\cdot}_{aq}$ concentration decreases by a factor of ~10^3, while the flux intensity decreases by a factor of ~10^5). Therefore, there are other sources of $OH^{\cdot}_{aq}$, which are the bulk chemical reaction (10A) and the photochemical reaction (37A) (Tables 2, 3).

Let us first consider the data referring to small drops. According to our calculations, the absolute concentration of hydroxyl radicals in these drops is

[3] The variation of the concentrations of atmospheric components in the gas and liquid phases is described by the equations

$$\frac{dC_g}{dt} = P_g - S_g - \left(C_g - \frac{C^{*G}_{aq}}{K_H L R^g T}\right) L k_t,$$

$$\frac{dC^G_{aq}}{dt} = P^G_{aq} - S^G_{aq} + \left(C_g - \frac{C^{*G}_{aq}}{K_H L R^g T}\right) L k_t,$$

where C_g is the concentration of a given component in the gas phase (molecules per cubic centimeter of cloud), P_g and S_g are the total formation and consumption rates of the component in the gas-phase reactions (molecules (cm^3 cloud)$^{-1}$ s^{-1}), P^G_{aq} and S^G_{aq} are the total formation and consumption rates of the component in the liquid-phase reactions (cm^{-3} s^{-1}), C^{*G}_{aq} is the component concentration on the drop surface (in 1 cm^3 of cloud), $K_H(i)$ is the Henry constant (mol l^{-1} atm^{-1}), R^g is the universal gas constant (0.082 l atm mol^{-1} K^{-1}), T is temperature (K), and k_t is the transfer coefficient (s^{-1}). As in an earlier study [10], it was assumed that $k_t = \left[\frac{r_i^2}{3D_g(i)} + \frac{4r_i}{3\bar{\omega}_i\alpha_i}\right]^{-1}$, where $D_g(i)$ is the diffusion coefficient in the gas phase (cm^2/s), $\bar{\omega}_i$ is the mean thermal velocity of molecules in the gas (cm/s), and α_i is the dimensionless accommodation coefficient. The gas–liquid chemical reactions are accompanied by acid–base processes, hydrolysis, and complexation in the drop phase. In the calculation of the equilibria in these processes, the set of liquid-phase reactions is augmented with the corresponding forward and reverse reactions. The ratio of their rate constants is taken to be equal to the equilibrium constant of the acid–base or another liquid-phase process [10].

[4] The contribution from the reactions involving $NO^{\cdot}_{3(aq)}$ is many times smaller than the contribution from the reactions of $OH^{\cdot}_{aq}$ because of the low concentration of nitrate radicals in the gas phase in the daytime. For this reason, the observed effects are hereafter ascribed to the reactions involving $OH^{\cdot}_{aq}$ and ozone, although the reactions involving $NO^{\cdot}_{3(aq)}$ are also taken into consideration.

Table 4. Dissociation equilibria in water drops

No.	Equilibrium	$K_{i\mathrm{E}}$, mol/l	Forward		Reverse	
			$\vec{A}_{298}$, $\frac{\mathrm{l}^{-(n-1)}}{\mathrm{mol}^{-(n-1)}\,\mathrm{s}}$	$\vec{E}_\mathrm{a}/R$, K	$\overleftarrow{A}_{298}$, $\frac{\mathrm{l}^{-(n-1)}}{\mathrm{mol}^{-(n-1)}\,\mathrm{s}}$	$\overleftarrow{E}_\mathrm{a}/R$, K
1E*	$CO_{2(aq)} + H_2O \rightleftharpoons H_2CO_{3(aq)}$	7.7×10^{-7}	4.3×10^{-2}	9250	5.6×10^{4}	8500
2E	$H_2CO_{3(aq)} \rightleftharpoons H^+_{aq} + HCO^-_{3(aq)}$	4.3×10^{-7}	2.15×10^{4}	–	5×10^{10}	–
3E	$H_2O \rightleftharpoons H^+_{aq} + OH^-_{aq}$	1.8×10^{-16}	2.34×10^{-5}	6800	1.3×10^{11}	–
4E	$H_2SO_{4(aq)} \rightleftharpoons HSO^-_{4(aq)} + H^+_{aq}$	1.0×10^{2}	5.0×10^{12}	–	5×10^{10}	–
5E	$HCO^-_{3(aq)} \rightleftharpoons H^+_{aq} + CO^{2-}_{3(aq)}$	4.7×10^{-11}	2.35	1820	5×10^{10}	–
6E	$HNO_{2(aq)} \rightleftharpoons H^+_{aq} + NO^-_{2(aq)}$	5.3×10^{-4}	2.65×10^{-7}	1760	5×10^{10}	–
7E	$HNO_{3(aq)} \rightleftharpoons H^+_{aq} + NO^-_{3(aq)}$	22	1.1×10^{12}	–1800	5×10^{10}	–
8E	$HNO_{4(aq)} \rightleftharpoons H^+_{aq} + NO^-_{4(aq)}$	1.0×10^{-5}	5.0×10^{5}	–	5×10^{10}	–
9E	$HO^{\bullet}_{2(aq)} \rightleftharpoons O^{-\bullet}_{2(aq)} + H^+_{aq}$	1.6×10^{-5}	8.0×10^{5}	–	5×10^{10}	–
10E	$HSO^-_{3(aq)} \rightleftharpoons H^+_{aq} + SO^{2-}_{3(aq)}$	6.22×10^{-8}	3110	–1960	5×10^{10}	–
11E	$HSO^-_{4(aq)} \rightleftharpoons H^+_{aq} + SO^{2-}_{4(aq)}$	1.02×10^{-2}	1.02×10^{9}	–2700	1×10^{11}	–
12E	$HSO^-_{5(aq)} \rightleftharpoons H^+_{aq} + SO^{2-}_{5(aq)}$	4.0×10^{-10}	20	–	5×10^{10}	–
13E**	$SO_{2(aq)} + H_2O_{aq} \rightleftharpoons HSO^-_{3(aq)} + H^+_{aq}$	3.1×10^{-4}	6.27×10^{4}	–1940	2×10^{8}	–

Note: $K_{i\mathrm{E}}$ is the equilibrium constant, n is the reaction order, $\vec{A}_{298}$ and $\vec{E}_\mathrm{a}$ are the preexponential factor at 298 K and the activation energy of the forward reaction, and $\overleftarrow{A}_{298}$ and $\overleftarrow{E}_\mathrm{a}$ are the preexponential factor at 298 K and the activation energy of the reverse reaction.

* $K_{i\mathrm{E}}$ has dimensions of l/mol.

** K_E is dimensionless.

$\overline{[OH^{\bullet}_{aq}]}_{r_0 = 0.1\ \mu m} \approx 2.1 \times 10^{-12}$ mol/l (Fig. 1a). Accordingly, the probability of these radicals being entrained is $\gamma_{OH(r_0 = 0.1\ \mu m)} = (1 - \overleftarrow{\Psi}_{OH}/\vec{\Psi}_{OH}) \approx w_{5A}/\vec{\Psi}_{OH} \approx 3.3 \times 10^{-3}$, where $\vec{\Psi}_{OH}$ and $\overleftarrow{\Psi}_{OH}$ are the hydroxyl fluxes from the gas to the liquid and vice versa, respectively. This γ_{OH} value is more than one order of magnitude smaller than the $OH^{\bullet}_g$ accommodation coefficient ($\alpha_{OH} = 5 \times 10^{-2}$ [10]). Most of the $OH^{\bullet}_g$ radicals impinging on the drop surface leave the drops to return to the gas phase. Their penetration into the drop is limited by the hydroxyl solubility. Indeed, the characteristic time of the establishment of a local (surface) thermodynamic hydroxyl solution equilibrium is $\overleftarrow{\tau}_{OH} = D_{aq}(OH^{\bullet})(4K_H(OH^{\bullet}_g)R^gT/\alpha_{OH}\bar{\omega}_{OH})^2 \approx 10^{-5}$ s. This time is sufficient for the $OH^{\bullet}_{aq}$ radicals to diffuse to a depth no higher than $\Delta_{OH} \approx (D_{aq}(OH^{\bullet}_{aq})\overleftarrow{\tau}_{OH})^{1/2} \approx 10^{-5}$ cm [9]. From this very thin layer, which is saturated to equilibrium, $OH^{\bullet}_{aq}$ radicals diffuse into the free volume of the drop. The uniformity of their distribution in the drop is governed by the ratio between the reaction length $l_{OH} = \xi^{-1}_{4A/5A} = (D_{aq}(OH^{\bullet})/k_{5A}[HSO^-_{3(aq)}](1 + k_{4A}K_{10E}/k_{5A}[H^+_{aq}]))^{1/2}$ (the distance traveled by a hydroxyl radical during its lifetime) and r_0. Under the

conditions examined, $l_{OH} \approx (D_{aq}(OH^{\bullet})\tau_{5A})^{1/2} \approx 1$ μm (Tables 1, 2, 4). Therefore, reactions (4A) and (5A) can cause a decrease in the equilibrium $OH^{\bullet}_{aq}$ concentration only in drops larger than 1 μm ($q_{OH} = l_{OH}/r_0 < 1$). This inference is confirmed by comparing the calculated near-surface and bulk concentrations of these species, which are, respectively, $[OH^{\bullet}_{aq}]_{surf} = 10^3 K_H(OH^{\bullet}_g)R^g T[OH^{\bullet}_g]/N_A \approx 2 \times 10^{-12}$ mol/l and $\overline{[OH^{\bullet}_{aq}]} \approx 2.1 \times 10^{-12}$ mol/l (Fig. 1a).[5] The similarity of these concentrations is evidence that the $OH^{\bullet}_{aq}$ radicals entrained from the gas are uniformly distributed throughout the volume of a small drop. However, it does not follow from the above that the $OH^{\bullet}_{aq}$ loss reactions (4A) and (5A) do not occur in small drops. Conversely, these reactions in small drops proceed at the highest rate, since the concentration of $OH^{\bullet}_{aq}$ radicals involved in these reactions is close to its equilibrium value (Fig. 1a). Accordingly, the contribution from $OH^{\bullet}_g$ entrainment to sulfur dioxide oxidation is the largest in the case of small drops; however, $\vec{\Psi}_{OH}/(w_{4A} + w_{5A}) \gg 1$ and $\overleftarrow{\Psi}_{OH}/(w_{4A} + w_{5A}) \gg 1$. The above-noted $OH^{\bullet}_{aq}$ concentration plateau at drop sizes below 1 μm (Fig. 1a) is the graphical implication of these inequalities. For larger drops ($r_0 \approx 1$ μm, $q_{OH} \approx 1$), reactions (4A) and (5A) would be expected to dominate over $OH^{\bullet}_{aq}$ diffusion and, accordingly, the surface (equilibrium) concentration of hydroxyl radicals would be expected to differ from the drop-average concentration: $[OH^{\bullet}_{aq}]_{surf}/\overline{[OH^{\bullet}_{aq}]} \geq 1$. Here, it is necessary to remember the other sources of hydroxyl radicals, namely the chemical reaction (10A) and the photochemical reaction (37A) (Tables 2, 3). The effect of these reactions on $[OH^{\bullet}_{aq}]$ will be clear if our calculated data are compared to the analytically found distribution of the concentration of an entrained model reagent in the drop [9].[6] Schwartz and Freiberg [9] found the steady-state distribution of this reagent in the drop by solving the diffusion equation. It was assumed that the reagent is consumed only through a first-order reaction. The $OH^{\bullet}_{aq}$ radicals in our model are consumed in the same way, because $\overline{[OH^{\bullet}_{aq}]} \ll [SO^{2-}_{3(aq)}]$ and $\overline{[OH^{\bullet}_{aq}]} \ll [HSO^{-}_{3(aq)}]$. It can therefore be assumed that the consumption of these species in the bimolecular reactions (4A) and (5A) obeys a first-order rate law. Our calculations lead to $([OH^{\bullet}_{aq}]_{surf}/\overline{[OH^{\bullet}_{aq}]}_{r_0 = 1\ \mu m}) \approx 1.08$. A similar result is obtained if data reported in [9] are used. Their identity is evidence of a minor role of processes (10A) and (37A) in $OH^{\bullet}_{aq}$ formation in micron-sized drops. The main source of $OH^{\bullet}_{aq}$ radicals in small drops is apparently the entrainment of these radicals from the gas phase. For $r_0 = 10$ μm, which is close to the size of the most abundant drops in a typical cloud,

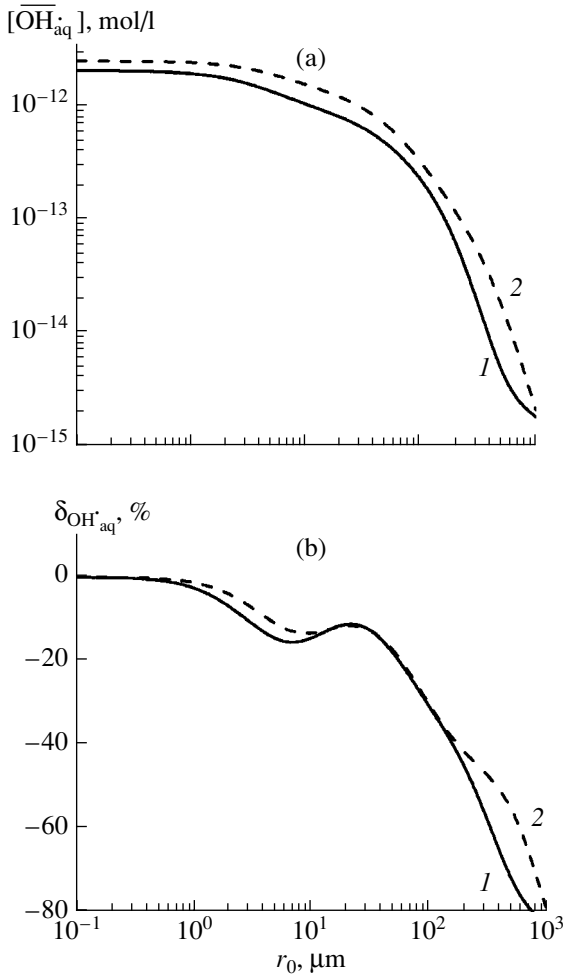

Fig. 1. Effect of the drop size in tropospheric clouds on (a) $[\overline{OH^{\bullet}_{aq}}]$ and (b) $\delta_{OH_{aq}}$ (see text) for $t_{ex} = (1)\ 10^3$ and $(2)\ 5 \times 10^3$ s (daytime). $L = 10^{-6}$. For the concentrations of gas components, see Table 1.

[5] The value $[OH^{\bullet}_{(g)}]^{t_{ex} = 10^3\ s}_{T_0 = 0.1\ \mu m} \approx 2 \times 10^6$ cm^{-3} is the hydroxyl concentration in the gas phase.

[6] This comparison between calculated data will be correct if the changes in the rates of the liquid-phase processes due to r_0 variation do not cause radical changes in the gas phase concentration of the reagent. According to our calculations, an increase in the drop size from 0.1 to 10 mm causes only a small (15%) increase in the $OH^{\bullet}_g$ concentration. A similar increase in $[\overline{OH^{\bullet}_{aq}}]$ in passing from small to larger drops was noted in [8].

our calculations lead to $([OH^{\cdot}_{aq}]_{surf}/\overline{[OH^{\cdot}_{aq}]}_{r_0 = 10\ \mu m}) \approx 2.6$. According to Schwartz and Freiberg [9], the same ratio between the surface and drop-average concentrations of the model reagent is ~7. This difference between the concentration ratios suggests that, in our case, there are other sources of $OH^{\cdot}_{aq}$ in the drops (that is, reactions (10A) and (37A) take place). The same is evident from Fig. 1b. The curves shown in Fig. 1b represent the results of our calculations concerning the effect of the nonuniformity of $\overline{[OH^{\cdot}_{aq}]}$ and $O_{3(aq)}$ distribution in the drop bulk on $\overline{[OH^{\cdot}_{aq}]}$. This nonuniformity was characterized by the quantity $\delta_{OH} = \delta \times 100\%/[OH^{\cdot}_{aq}]$, where $\delta = \overline{[OH^{\cdot}_{aq}]} - [OH^{\cdot}_{aq}]$. The first term in this difference is equal to the $OH^{\cdot}_{aq}$ concentration calculated taking into account both the *S*/*V* factor and the $OH^{\cdot}_{aq}$ and $O_{3(aq)}$ distribution nonuniformity factor. The second term is equal to the $OH^{\cdot}_{aq}$ concentration calculated for the case of a uniform distribution of all components in the drop. In essence, Fig. 1b illustrates the difference between the $OH^{\cdot}_{aq}$ concentrations under the uniform and nonuniform $OH^{\cdot}_{aq}$ and $O_{3(aq)}$ distribution conditions as a function of drop size. It can be seen in Fig. 1b that an adverse effect of the $OH^{\cdot}_{aq}$ distribution nonuniformity is initially manifested. This effect is significant starting at $r_0 \approx 1$ μm ($\approx l_{OH}$). For $r_0 = 5$ μm, taking into account this factor decreases $\overline{[OH^{\cdot}_{aq}]}$ by ~20% relative to the uniform distribution of hydroxyl radicals. The data presented in Fig. 1b are also in qualitative agreement with our data concerning the effect of processes (10A) and (27A) on $\overline{[OH^{\cdot}_{aq}]}$. In particular, it is clear that, for the smallest drops, the decrease in the $OH^{\cdot}_{aq}$ concentration due to the near-surface reactions (4A) and (5A) is not compensated for by the chemical and photochemical generation of $OH^{\cdot}_{aq}$ in the drop bulk. The effect of these processes on $\overline{[OH^{\cdot}_{aq}]}$ is manifested starting at a much larger drop size (Fig. 1b). This is indicated by the decrease in the descent rate of the $OH^{\cdot}_{aq}$ concentration at $r_0 = 7$–8 μm in a growing drop. The slight descent is followed by an ascending portion of the curve in spite of the decreasing $OH^{\cdot}$ "permeability" of the drop. Calculations have demonstrated that the maximum in the $\delta_{OH} = f(r_0)$ curve is solely due to reaction (10A). Furthermore, it follows from Fig. 1b that the effect of this reaction persists up to $r_0 \approx 25$–30 μm, after which $\overline{[OH^{\cdot}_{aq}]}$ decreases again. This is caused by the deceleration of reaction (10A) due to its near-surface localization; $l_{O_3} = (D_{aq}/k_{10A}[\overline{O^{-\cdot}_{2(aq)}}])^{1/2} \approx 50$ μm (Fig. 1b). Indeed, reaction (10A) somewhat raises $\overline{[OH^{\cdot}_{aq}]}$ in larger drops as well. This is indicated, for example, by the above-mentioned disagreement between the descent rate of the $OH^{\cdot}_{aq}$ concentration and the decrease in $\vec{\Psi}_{OH}$. However, the rate of this reaction in large drops is insufficiently high to compensate for the unfavorable effect of ozone consumption in the subsurface layer of the drop. The contribution from the photolysis of dissolved hydrogen peroxide to $OH^{\cdot}_{aq}$ generation is also small. The effect of this process is observed only in the largest drops, when the $OH^{\cdot}_{g}$ and $O_{3(g)}$ fluxes are almost exhausted. This is indicated by a comparison between the calculated $\vec{\Psi}_{OH}$ values and the rates of reactions (10A) and (37A) (Tables 2, 3). For example, for $r_0 = 10^2$ μm, $\vec{\Psi}_{OH} \approx 1.7 \times 10^4$ cm^{-3} s^{-1}. Under these conditions, $w_{10A} \approx 2 \times 10^5$ cm^{-3} s^{-1} and $w_{37A} \approx 1.6 \times 10^4$ cm^{-3} s^{-1}; i.e., $w_{10A} + 2w_{37A} \approx 2.3 \times 10^5$ cm^{-3} s^{-1} ($\gg \vec{\Psi}_{OH}$) and $w_{10A}/w_{37A} \gg 1$.

$HO^{\cdot}_{2(aq)}$ Radical

The drop size effect on the sum of the $HO^{\cdot}_{2(aq)}$ and $O^{-\cdot}_{2(aq)}$ concentrations (hereafter designated $\overline{[HO^{\cdot}_{2(aq)}]}$ for brevity) is illustrated in Fig. 2a. As in the case of $OH^{\cdot}_{aq}$, the data obtained reflect the overall effect of two factors on $\overline{[HO^{\cdot}_{2(aq)}]}$, namely, the *S*/*V* factor and the nonuniformity of the bulk distribution of $OH^{\cdot}_{aq}$ and $O_{3(aq)}$ due to their near-surface reactions. Calculations have demonstrated that, unlike the reactions involving $OH^{\cdot}$, the liquid-phase reactions involving $HO^{\cdot}_{2(aq)}$ markedly reduce the concentration of these radicals in the gas phase. Most of these species in clouds are lost through liquid-phase reactions. A comparison between the plots shown in Figs. 1a and 2a suggests that, although these plots seem to be similar, the $\overline{[HO^{\cdot}_{2(aq)}]}$ plateau is dozens of times as long as the $OH^{\cdot}_{aq}$ plateau. Note also that, although $\vec{\Psi}_{HO_2}$ and $\vec{\Psi}_{OH}$ are similar, the species concentration ratio in the plateau region (i.e., $(\overline{[HO^{\cdot}_{2(aq)}]} + \overline{[O^{-\cdot}_{2(aq)}]})/\overline{[OH^{\cdot}_{aq}]}$) is as large as ~$10^4$. The

rate of $[\overline{HO^{\cdot}_{2(aq)}}]$ decline is approximately one order of magnitude lower than the rate of the decrease in the intensity of the $HO^{\cdot}_{2(g)}$ flux into the drop ($\vec{\Psi}_{HO_2}$). Since there are no $HO^{\cdot}_{2(aq)}$ sources in the drops (see Table 2), this fact means that, firstly, the growth of the drops is accompanied by a decrease in the loss rate of $HO^{\cdot}_{2(aq)}$ and, secondly, the determining factor in the loss of this species is the quadratic-law reactions (1A) and (2A). From the data presented in Fig. 2a, it can be found that the probability of $HO^{\cdot}_{2(g)}$ being entrained by the finest drops is close to the same probability for $OH^{\cdot}_{g}$: $\gamma_{HO_2(r_0 = 0.1\ \mu m)} = (1 - \overleftarrow{\Psi}_{HO_2}/\vec{\Psi}_{HO_2}) \approx 4 \times 10^{-3}$. The calculated probability is, however, only ~2.5 times lower than the α_{HO_2} value accepted in calculations [10]. Evidently, the dynamics of $HO^{\cdot}_{2(g)}$ entrainment by the finest drops is determined by chemical reactions in the liquid phase. The above facts are due to the difference between the reactivities and solubilities of $OH^{\cdot}$ and $HO^{\cdot}_2$ [1]. The $HO^{\cdot}_{2(aq)}$ radical, which is less reactive, participates in the recombination reactions (1A), (2A), (17A), and (18A), along with being consumed in reaction (10A) according to a linear rate law. Drop growth causes changes not only in absolute reaction rates but also in the ratios of these rates. Above the critical size ($q_{OH} \approx 1$), reactions (1A) and (2A) will dominate in their competition with reactions (17A) and (18A). This is a consequence of reactions (4A) and (5A) occurring on the surface, which result in a dramatic decrease in the $SO^{-\cdot}_{5(aq)}$ generation rate and, accordingly, in the rates of reactions (17A) and (18A): $(w_{17A} + w_{18A})/(w_{1A} + w_{2A}) \approx 1 : 0.7$. Furthermore, the increase in the rates of reactions (1A) and (2A) diminishes the role of reaction (10A): above the critical drop size, the $w_{10A}/(w_{1A} + w_{2A})$ ratio decreases steadily. For larger drops, the competition between reactions (1A) and (2A) and reactions (17A) and (18A) is also affected by the bulk chemical reaction (10A) and the bulk photochemical reaction (37A) (see above). For example, for $r_0 = 10\ \mu m$ ($\vec{\Psi}_{HO_2}/\vec{\Psi}_{OH})_{r_0 = 10\ \mu m} \approx 10$), $(w_{17A} + w_{18A})/(w_{1A} + w_{2A}) \approx 1 : 3.2$. Since the hydroperoxyl radical is more soluble than $OH^{\cdot}$, it takes a longer time to reach the equilibrium hydroperoxyl saturation of a drop. Accordingly, the hydroperoxyl radical penetrates deeper into the drop: $\Delta_{HO_2} \approx (D_{aq}\overleftarrow{\tau}_{HO_2})^{1/2} \approx 4 \times 10^{-2}$ cm. Comparing this value with the reaction length for this species, $l_{HO_2} = (D_{aq}/k^*_{17A})^{1/2} \approx 6 \times 10^{-3}$ cm, we obtain $\Delta_{HO_2}/l_{HO_2} \gg 1$; that is, the dissolution of $HO^{\cdot}_{2(g)}$ species is inevitably accompanied by their loss. Here, $(k^*_{17A})^{-1} = (k_{17A}[SO^{-\cdot}_{5(aq)}])^{-1} + (k_{18A}[SO^{-\cdot}_{5(aq)}])^{-1} = 2(k_{17A}[SO^{-\cdot}_{5(aq)}])^{-1}$. As a consequence, the equilibrium liquid-phase concentration of these species calculated using the Henry law, $[HO^{\cdot}_{2(aq)}] = 10^3 \times K_H(HO^{\cdot}_{2(g)})R^gT[HO^{\cdot}_{2(g)}]/N_A \approx 1.5 \times 10^{-8}$ mol/l, is not reached under atmospheric conditions. This is also indicated by computer-calculated data (Fig. 2a): the calculated $HO^{\cdot}_{2(aq)}$ and $O^{-\cdot}_{2(aq)}$ concentrations are approximately 1.5 times lower than the equilibrium concentrations.

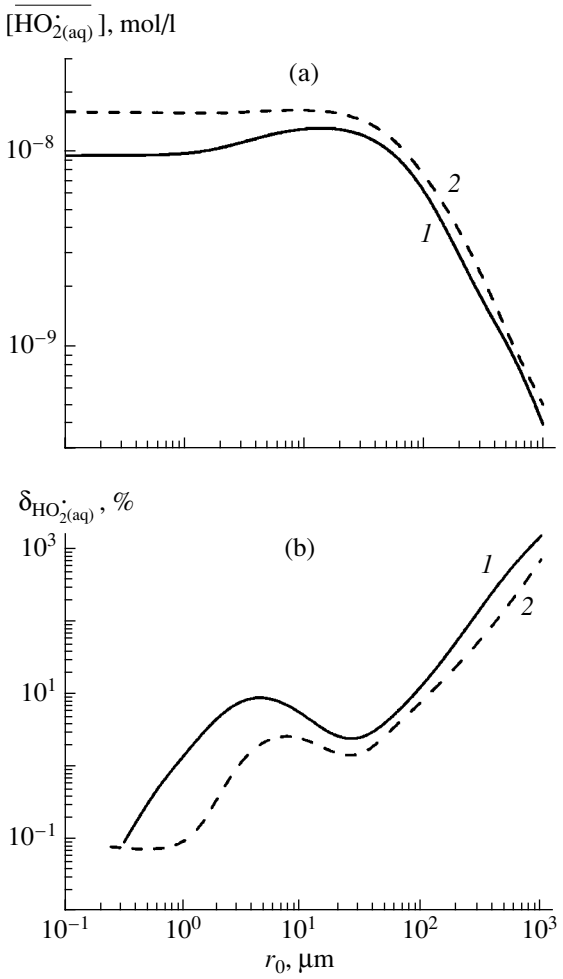

Fig. 2. Effect of the drop size in tropospheric clouds on (a) $[\overline{HO^{\cdot}_{2(aq)}}]$ and (b) $\delta_{HO^{\cdot}_{2(aq)}}$ (see text) for t_{ex} = (*1*) 10^3 and (*2*) 5×10^3 s (daytime). $L = 10^{-6}$.

Calculations have demonstrated that the effect of chemical reactions on $[\overline{HO^{\cdot}_{2(aq)}}]$ is more pronounced for shorter exposure times (Fig. 2a). For micron-sized

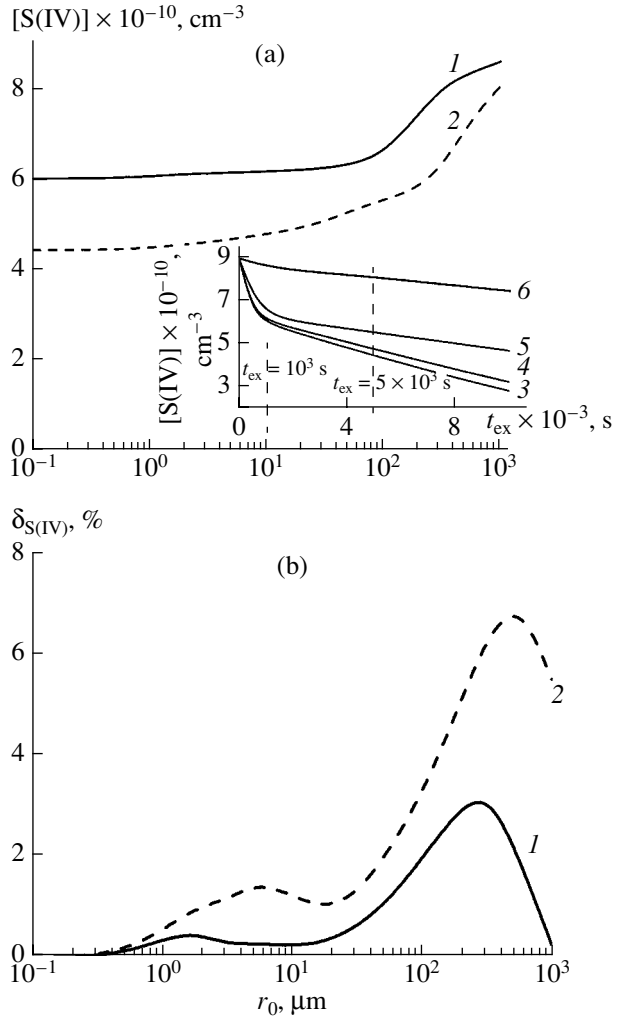

Fig. 3. Drop size effect on (a) the concentration of unreacted sulfur dioxide $[S(IV)]_t$ and (b) $\delta_{S(IV)}$ (see text) for t_{ex} = (*1*) 10^3 and (*2*) 5×10^3 s (daytime). $L = 10^{-6}$, the initial $SO_{2(g)}$ concentration is 3.5 ppb, and the initial H_2O_2 concentration is 1 ppb. The inset shows the time variation of $[S(IV)]_t$ for drop sizes of (*3*) 1, (*4*) 10, (*5*) 10^2, and (*6*) 10^3 μm.

drops, shortening the exposure time causes a nearly twofold decrease in the $HO^{\cdot}_{2(aq)}$ concentration because of reactions (1A) and (2A) proceeding at a higher rate.[7] At first glance, it might seem that the adverse effect of these reactions on $[\overline{HO^{\cdot}_{2(aq)}}]$ does not extend to larger drops (Fig. 2a). Indeed, the $[\overline{HO^{\cdot}_{2(aq)}}]_{t_{ex} = 10^3} = f(r_0)$ plot shows an ascent as the drop size is increased. The cause of this apparent contradiction is the retardation of the cross recombination ($HO^{\cdot}_{2(aq)}/O^{-\cdot}_{2(aq)} + SO^{-\cdot}_{5(aq)}$) (reactions (17A) and (18A)) due to the consumption of $OH^{\cdot}_{aq}$ radicals near the surface. It is due to the resulting "economy" in $HO^{\cdot}_{2(aq)}/O^{-\cdot}_{2(aq)}$ that, in spite of the higher loss rate of these species (reactions (1A), (2A), and (10A)) and in spite of the decrease in $\vec{\Psi}_{HO_2}$, the concentration of these species increases as the drops grow at $t_{ex} = 10^3$ (Fig. 2a).

A measure of the indirect effect of the nonuniformity of $OH^{\cdot}_{aq}$ and $O_{3(aq)}$ distribution in the drop bulk on $[\overline{HO^{\cdot}_{2(aq)}}]$ is the quantity δ_{HO_2} (Fig. 2b).[8] For comparatively small drops ($r_0 \le 5$ μm), calculations indicate only a slight increase in the $HO^{\cdot}_{2(aq)}$ concentration ($\delta_{HO_2} \approx 10\%$), which is due to the above-mentioned retardation of reactions (17A) and (18A). For large drops, the surface localization of the reactions involving $OH^{\cdot}$ and O_3 exerts a much stronger effect on $[\overline{HO^{\cdot}_{2(aq)}}]$. For example, $\delta_{HO_2} \approx 100\%$ for $r_0 = 300$ μm and 1000% for $r_0 = 10^3$ μm. The dramatic strengthening of this effect is obviously due to the fact that the absolute rates of liquid phase reactions are much lower in large drops. Calculations have demonstrated that the rate of reaction (10A) in gas volume terms is 2×10^5 cm^{-3} s^{-1} for $r_0 = 10^2$ μm and is almost two orders of magnitude lower for $r_0 = 10^3$ μm. As a consequence, even comparatively small changes in the concentrations of $OH^{\cdot}_{2(aq)}$ and $O_{3(aq)}$ due to a decrease in the flux of these species from the gas phase, as well as variations in the rate of reaction (10A), cause large changes in $[\overline{HO^{\cdot}_{2(aq)}}]$.

Sulfur Dioxide

The self-cleaning of the atmosphere from sulfur dioxide in the absence of water drops is a rather slow process [1, 21]. For an $SO_{2(g)}$ concentration of ~3.5 ppb, the self-cleaning rate does not exceed ≈0.04 ppb/h (1%/h) [12]. Water drops markedly intensify the process, as is demonstrated in the inset in Fig. 3a. The

[7] According to calculated data, the increase in r_0 at small t_{ex} values slows down $SO_{2(g)}$ oxidation. In the absence of buffer admixtures, $pH_{r_0 = 20–30\ \mu m}/pH_{r_0 = 0.1\ \mu m} > 1$. As a consequence, the equilibrium $HO^{\cdot}_{2(aq)} \rightleftharpoons H^+ + O^{-\cdot}_{2(aq)}$ (9E) (Table 4) is shifted to the right and the rate of reaction (2A) increases rapidly, implying a decline in the calculated $[\overline{HO^{\cdot}_{2(aq)}}]$ value.

[8] δ_{HO_2} was calculated in the same way as δ_{OH}.

$[S(IV)]_t = f(t)$ plot presented here shows how the concentration of unreacted sulfur dioxide, including the species dissolved in water, varies with time. Here, $[S(IV)]_t = [SO_{2(g)}]_t + [\text{sulfite}]_t N_A L/10^3 \approx [SO_{2(g)}]_t + [HSO^-_{aq}]_t N_A L/10^3$. For $r_0 = 1$ μm and $L = 10^{-6}$, the time-average self-cleaning rate, including the liquid-phase reactions, is ~2 ppb/h (50%/h) [11]. In the calculation of $[S(IV)]_t$, we took into account the S/V factor and the near-surface consumption of $OH^{\cdot}_{2(aq)}$ and $O_{3(aq)}$. This strong effect of water drops on $SO_{2(g)}$ oxidation is obviously due to the fact that liquid-phase sulfite oxidation reactions are included in the calculation [2, 22, 23]. Therefore, the contribution from these reactions can be viewed as a characteristic of the oxidizing properties of cloud drops with respect to sulfur dioxide absorbed from the gas phase. It is clear from the curves presented in the inset in Fig. 3a that $[S(IV)]_t$ decreases nonuniformly with time: the process has a rapid and a slow stage. The former is observed for $t_{ex} \le 10^3$ s; the latter, for $t_{ex} > 10^3$ s. As the drops grow, the kinetic difference between the rapid and slow stages vanishes against the background of the slowdown of $SO_{2(g)}$ oxidation. This is evident from the $[S(IV)]_t = f(r_0)$ plots for $t_{ex} = 10^3$ and 5×10^3 s (Fig. 3a, vertical dashed marks in the inset). At $r_0 > 100$ μm, there is a well-defined slowdown of $SO_{2(g)}$ oxidation (an increase in the concentration of unreacted $SO_{2(g)}$ and its ionic forms).

In an earlier work [12], we demonstrated that the rapid stage of self-cleaning is hydrogen peroxide transport from the gas phase followed by the liquid-phase reaction $H_2O_{2(aq)} + HSO^-_{3(aq)}$ (3A); here, $\Delta[S(IV)]_{t_{ex} = 10^3} \approx [H_2O_{2(g)}]_{t_{ex} = 0} \approx 2.7 \times 10^{10}$ cm^{-3} (Table 1). The self-cleaning route due to ozone influx is much less pronounced. At $t_{ex} = 10^3$ s, it accounts for no more than 2% of the reacted $SO_{2(g)}$. At this time point, nearly all of the ozone in the gas phase is reacted. Nevertheless, the self-cleaning of the gas from $SO_{2(g)}$ is not terminated (Fig. 3a). Therefore, other oxidation processes also occur in the drops. It is surprising that, after $H_2O_{2(g)}$ is exhausted, the reaction between hydrogen peroxide and sulfite (3A) continues to play a significant role in $[SO_{2(g)}]$ diminution and in the slow stage. The source of $H_2O_{2(aq)}$ under these conditions is the recombination of $HO^{\cdot}_{2(aq)}$ and $O^{-\cdot}_{2(aq)}$ radicals (reactions (1A) and (2A)). According to our calculations, the contribution from $SO_{2(g)}$ oxidation with oxygen also becomes significant. In small drops, this process is initiated by the entrainment of hydroxyl radicals from the gas phase: $OH^{\cdot}_{aq} + SO^{2-}_{3(aq)}/HSO^-_{3(aq)}$ (reactions (4A) and (5A)). The process involving $SO^{-\cdot}_{3-5(aq)}$ develops through reactions (12A), (17A), and (18A) and ends as reaction (6A). Thus, at the slow stage of self-cleaning, the oxidizing properties of small drops with respect to $SO_{2(g)}$ are influenced by the influx of $OH^{\cdot}_g$ and $HO^{\cdot}_{2(g)}$ from the gas phase.[9] It is, therefore, clear why the self-cleaning rate in the slow stage decreases as the drops grow (Fig. 3a). This effect is caused by the decrease in the rates of liquid-phase reactions involving hydrogen peroxide and these radicals due to a decrease in the flux of these species into the drops. The contributions from the peroxide and radical entrainment routes to $SO_{2(g)}$ oxidation depend on both r_0 and t_{ex}. For small drops ($r_0 \le 1$ μm) and $t_{ex} = 5 \times 10^3$ s, up to ~60% of the sulfur dioxide is converted via the oxygen route. For larger drops, for example, those with $r_0 = 10^2$ μm, the contribution from the oxygen route of oxidation does not exceed ~30%. This is due to the adverse effect of the S/V factor and of the nonuniformity of the rates of the reactions involving $OH^{\cdot}_{aq}$ and $O_{3(aq)}$ in the drop bulk. A clear notion of the size effects in the formation of $SO_{2(g)}$ oxidation properties of the drops is provided by Fig. 3b. Here, the measure of these effects is $\delta_{S(IV)}$. This quantity was calculated in the same way as δ_{OH} and δ_{HO_2}: $\delta_{S(IV)} = \delta 100\%/[S(IV)]$. Drop growth, which increases the role of the near-surface consumption of $OH^{\cdot}_{aq}$ and $O_{3(aq)}$, may seem to exert only a slight effect on $[S(IV)]_t$. The $\delta_{S(IV)}$ value calculated for short exposure times is no greater than ~3% even for the largest drops. This result is in agreement with the data indicating that hydrogen peroxide arriving from the gas phase plays the dominant role in $SO_{2(g)}$ oxidation (Fig. 3a). However, the adverse effect of the near-surface reactions of $OH^{\cdot}_{aq}$ and $O_{3(aq)}$ in the formation of the oxidizing properties of the drops is obvious even under these "unfavorable" conditions. Note that the $\delta_{S(IV)}$ data plotted here mask the actual slowdown of $SO_{2(g)}$ oxidation due to the near-surface reactions of $OH^{\cdot}_{aq}$ and $O_{3(aq)}$, because they inevitably involve a number of compensation effects. For example, as the drop size grows from 1 to 10 μm, a

[9] For short exposure times, the self-cleaning of the atmosphere from $SO_{2(g)}$ due to the influx of $H_2O_{2(g)}$ dominates over the other self-cleaning routes for all r_0. This is indicated by the inflection at $r_0 \ge 150$ mm in the curve shown in Fig. 3a. The characteristic time of $H_2O_{2(g)}$ diffusion from the gas into the drop, $\tau_{diff}(H_2O_{2(g)})$, which is proportional to r_0^2, is longer than $t_{ex} = 10^3$ s under these conditions. As a consequence, further drop growth causes the sulfur dioxide consumption to decrease roughly following the law $\Delta[S(IV)]_t \approx [H_2O_{2(g)}]t_{ex}/\tau_{diff}(H_2O_{2(g)}) \sim 1/r_0^2$. As the drop size increases, the concentration of unreacted sulfur dioxide, including dissolved ionic forms, approaches nearer and nearer to its initial value, $[S(IV)]_{t_{ex} = 0}$ (Fig. 3a).

nearly twofold decrease in the rates of reactions (5A) and (6A) is accompanied by a nearly equal increase in the rates of reactions (1A)–(3A). It is also essential that the effect of the near-surface reactions is considered for a high rate of SO_2 influx from the gas phase. Therefore, a decrease in the SO_2 concentration must cause an increase in $\delta_{S(IV)}$. This indirectly indicates that $\delta_{S(IV)}$ grows in passing from $t_{ex} = 10^3$ to 5×10^3 s (Fig. 3b). This deduction is confirmed by direct calculations: for micron-sized drops and $t_{ex} = 5 \times 10^3$ s, a doubled $\delta_{S(IV)}$ value is obtained for an $SO_{2(g)}$ concentration of 1.75 ppb.

Another interesting feature is that $\delta_{S(IV)}$ varies nonmonotonically as the drops grow. The plots in Fig. 3b indicate local dips in the $SO_{2(g)}$ oxidation ability of the drops. The first dip (for $t_{ex} = 10^3$ s) is observed at $r_{0(1)} \approx 1.5$ μm; the second, at $r_{0(2)} \approx 250$–300 μm. The first particle size is nearly equal to the calculated l_{OH} value. Since $OH^{\cdot}_{aq}$ radicals are uniformly distributed in micron-sized and smaller drops, the secondary species $SO^{-\cdot}_{3-5(aq)}$ and $HSO^{-}_{5(aq)}$, which enhance the oxidizing properties of the drops, are also uniformly distributed there. In particular, it is clear from the liquid-phase reactions presented in Table 2 that two sulfite molecules per $HSO^{-}_{5(aq)}$ species are oxidized (reaction (6A)). Therefore, reaction (6A) is suppressed in drops with a size larger than $r_{0(1)}$ (that is, under such conditions that the near-surface processes involving $OH^{\cdot}_{aq}$ proceed at high rates). As a consequence, sulfite consumption slows down and $\delta_{S(IV)}$ increases (Fig. 3b). This interpretation of the "fine structure" of the oxidizing properties of the drops is in qualitative agreement with the abovementioned finding that $\delta_{S(IV)}$ shifts to larger $r_{0(i)}$ values as t_{ex} is increased (Fig. 1b). Obviously, increasing t_{ex} leads to a higher $SO_{2(g)}$ conversion and, accordingly, a lower $[S(IV)]_t$ value (Fig. 3a). The increasing sulfur dioxide conversion acidifies the liquid phase in the drops. Equilibrium (13E) (Table 4) shifts to the left-hand side, the bisulfite ion concentration decreases, and l_{OH} increases. By examining the $\delta_{S(IV)}$ curve referring to $t_{ex} = 5 \times 10^{-3}$ (Fig. 3b) in the light of these considerations, we deduce that the $OH^{\cdot}_{aq}$ radicals penetrate to a depth of 1.5–2 μm under these conditions. This dramatic increase in the penetration depth is in agreement with the calculated change in the bisulfite ion concentration in the drops, specifically, $[HSO^{-}_{3(aq)}] \sim l^2_{OH}$. It is now clear why the oxidizing properties of the drops strengthen at $r_0 \geq 7$–8 μm (Fig. 3b). This effect is due to the generation of $\geqslant l_{OH}$ radicals (reaction (10A)) in the drop bulk. This process reinitiates sulfite consumption via the oxygen route: $O^{-\cdot}_{2(aq)} + O_{3(aq)} \xrightarrow[(10A)]{H^+} OH^{\cdot}_{aq} \xrightarrow[(5A),\,(12A),\,(17A)]{HSO^{-}_{3},\,O_2,\,HO^{\cdot}_{2}} HSO^{-}_{5(aq)} \xrightarrow[(6A)]{HSO^{-}_{3},\,H^+} 3H^+_{aq} + 2SO^{2-}_{4(aq)}$. This sulfite oxidation route, which is of secondary importance for the smallest drops, is crucial for larger drops.[10] The largest drop size for which the reinitiated oxygen route is still significant is apparently determined by the width of the near-surface ozone consumption zone: $l_{O_3} \approx 50$ μm (Fig. 3b). For drop sizes larger than l_{O_3}, a local weakening of the oxidation properties is again observed, which is indicated by a spike in the $\delta_{S(IV)}$ curve (Fig. 3b). The restrengthening of these properties at $r_0 \geq r_{0(2)}$ is due to the reinitiation of the oxygen route of liquid-phase $HSO^{-}_{3(aq)}$ oxidation. This time, $OH^{\cdot}_{aq}$ is provided by the photodissociation of $H_2O_{2(aq)}$ dissolved in water. For short exposure times, when the sulfur dioxide concentration in the gas phase can be taken to be constant, $l_{H_2O_2} = (D_{aq}(H_2O_{2(aq)})/k_{3A}[HSO^{-}_{3(aq)}]_{t_{ex}=0})^{1/2} \approx 3 \times 10^3$ μm. This estimate indicates that the $H_2O_{2(aq)}$ molecules arriving from the gas phase are uniformly distributed in the largest drops ($q_{H_2O_2} \ll 1$). The oxygen oxidation of sulfite proceeds according to the familiar scheme $H_2O_{2(aq)} \xrightarrow{h\nu} OH^{\cdot}_{aq} \xrightarrow[(5A),\,(12A),\,(17A)]{HSO^{-}_{3},\,O_2,\,HO_2} HSO^{-}_{5(aq)} \xrightarrow[(6A)]{HSO^{-}_{3},\,H^+} 3H^+_{aq} + 2SO^{2-}_{4(aq)}$.

Comparison with the Results of Field Experiments

In the framework of the GDF program, there was an integrated investigation into the dynamics and mechanisms of chemical processes in clouds supplemented with a study of the microphysics and chemical composition of aerosol particles and cloud drops, determination of the composition of atmospheric air, and weather monitoring [2]. One of the GDF subprojects included measuring the $SO_{2(g)}$ concentration along the wind direction, from the north foot of Great Dun Fell (Moorhouse, MH) through the summit (SU) to a site on the opposite side of the hill (Mine Road, MR) [22, 23]. A reliable indication of a decrease in $[SO_{2(g)}]$ upon con-

[10] The photolytic decomposition of the nitrite ion (reaction (38A)), nitrate ion (reaction (38A)), and hydrogen peroxide (reaction (37A)) do not contribute significantly to $OH^{\cdot}_{aq}$ formation under these conditions. For example, the contribution from hydrogen peroxide photolysis to $OH^{\cdot}_{aq}$ generation in drops with $r_0 = 10$ μm ($t_{ex} = 10^3$ s) is no greater than 1% of the contribution from the reaction $O^{-\cdot}_{2(aq)} + O_{3(aq)}$.

tact between polluted air and an orographic cloud[11] was obtained at the SU site on May 5, 9, and 10, 1993. For the cloud formation event on May 5, 1993 (from 7:00 p.m. to 9:00 p.m.), the average air self-cleaning rate was ≤1 ppb/h. From SU to MR, the volumetric liquid-water content changed from $(3.5 \pm 0.13) \times 10^{-7}$ to $(1 \pm 0.05) \times 10^{-7}$ and $[SO_{2(g)}]$ changed from 0.43 ± 0.43 to 0.37 ± 0.18 ppb; $[H_2O_{2(g)}]$ at the MR site was 0.32 ± 0.27 ppb. The correctness of the $SO_{2(g)}$ concentration measurements was confirmed by revealing a positive correlation between the increase in the sulfate ion concentration normalized with respect to the tracer (Na^+ ion) concentration ($[SO_4^{2-}]/[Na^+]$) and the $H_2O_{2(aq)}$ concentration. This correlation is evidence that, in the event considered, the oxidation of most of the $SO_{2(g)}$ involved hydrogen peroxide, since the $H_2O_{2(aq)}$ concentration in drops with $[S(IV)] \geq 10^{-5}$ mol/l was close to zero. In the cloud formation events on May 9 and 10, 1993, the time-average self-cleaning rate was 5 and 4 ppb/h, respectively.[12] Similar rates of air self-cleaning from $SO_{2(g)}$ were observed in earlier experiments [24], and they are close to the rate calculated in this work for the rapid self-cleaning stage, which is ~3.5 ppb/h ($[SO_{2(g)}] \approx 3.5$ ppb, $[H_2O_{2(g)}] = 1$ ppb, $L = 10^{-6}$, and $r_0 = 1$ μm). Agreement between the results of our calculations and the experimental data is also evident from the fact that the self-cleaning of atmospheric air on May 5, 1993, took a comparatively short time (a few minutes); that is, the key role in the process was played by $H_2O_{2(g)}$. Of particular interest are the results obtained with the use of an impactor separating aerosols into size fractions [22]. It was demonstrated that the increase in the normalized sulfate ion concentration $[SO_4^{2-}]/[Na^+]$ in aerosol particles, which was observed on May 5, 1993, is mainly due to liquid-phase $SO_{2(g)}$ oxidation. The authors of that study related this process to the in-cloud activation (spreading and subsequent dissolution) of dry aerosol particles with a size of 0.2–0.5 μm followed by their redrying.[13] However, it was impossible to reconstruct the size of the drops in which liquid-phase $SO_{2(g)}$ oxidation had taken place in the cloud, because the impactor did not allow drops to be discriminated according to their size. It was only found that most of the water collected had been 5-μm drops. Therefore, in that experimental study, the inference that liquid-phase $SO_{2(g)}$ oxidation occurs mainly in small drops could be made only from the short time taken by air self-cleaning.

[11] Orographic clouds result from the elevation and cooling of a humid air mass moving over a hilly or mountainous terrain.

[12] May 9, 1993: $[SO_{2(g)}] = 4.2 \pm 4.3$ ppb, $L = (4.6 \pm 1.5) \times 10^{-7}$ (SU); $[SO_{2(g)}] = 0.86 \pm 0.8$ ppb, $L = (1.6 \pm 0.6) \times 10^{-7}$ (MR). May 10, 1993: $[SO_{2(g)}] = 4.19 \pm 1.55$ ppb, $L = (7.2 \pm 1.3) \times 10^{-7}$ (SU); $[SO_{2(g)}] = 0.74 \pm 0.17$ ppb, $L = (2.4 \pm 1.2) \times 10^{-7}$ (MR).

[13] Although iron ions ($\sim 20 \times 10^{-9}$ g/m^3) were detected in the aerosol particles in parallel experiments [25], no positive correlation was observed between their concentration and the $SO_{2(g)}$ oxidation rate.

ACKNOWLEDGMENTS

This study was supported by the Presidium of the Russian Academy of Sciences through program no. 16, "Changes in the Environment and Climate—Natural Disasters."

REFERENCES

1. Warneck, P., Mirabel, V., Salmon, G.A., et al., in *Review of the Activities and Achievements of the EUROTRAC: Subproject HALIPP*, Warneck, P., Ed., Berlin: Springer, 1996, vol. 2, p. 7.
2. Choularton, T.W., Colville, R.N., Bower, K.N., et al., *Atmos. Environ.*, 1997, vol. 31, no. 16, p. 2393.
3. Seinfeld, J.H. and Pandis, S.N., *Atmospheric Chemistry and Physics: From Air Pollution to Climate Change*, New York: Wiley, 1998.
4. Ziajka, J., Beer, F., and Warneck, P., *Atmos. Environ.*, 1994, vol. 28, p. 2549.
5. Chameides, W.L. and Davis, D.D., *J. Geophys. Res.*, 1982, vol. 87, p. 4836.
6. Benkelberg, H.-J. and Warneck, P., *J. Phys. Chem.*, 1995, vol. 99, p. 5214.
7. Mauldine, R.L., Mandronich, S., Flocke, S.J., et al., *Geophys. Rev. Lett.*, 1997, vol. 24, p. 3033.
8. Jacob, D.J., *J. Geophys. Res*, 1986, vol. 91, p. 9807.
9. Schwartz, S.E. and Freiberg, J.E., *Atmos. Environ.*, 1981, vol. 15, p. 1129.
10. Herrmann, H., Ervens, B., Jacobi, H.-W., et al., *J. Atmos. Chem.*, 2000, vol. 36, p. 231.
11. Deguillaume, L., Leriche, M., Monod, A., et al., *Atmos. Chem. Phys. Discuss.*, 2003, vol. 3, p. 5019.
12. Ermakov, A.N., Larin, I.K., Ugarov, A.A., and Purmal', A.P., *Kinet. Katal.*, 2003, vol. 44, no. 4, p. 524 [*Kinet. Catal.* (Engl. Transl.), vol. 44, no. 4, p. 476].
13. Feigel'son, E.M., *Radiatsiya v oblachnoi atmosfere* (Radiation in the Cloudy Atmosphere), Leningrad: Gidrometeoizdat, 1981.
14. Isaac, G. and Schemenauer, R., *J. Appl. Meteorol.*, 1979, vol. 18, p. 1056.
15. Webster, P. and Stephens, G., *J. Atmos. Sci.*, 1980, vol. 37, p. 1521.
16. Telford, J.W. and Wagner, P.B., *Pure Appl. Geophys.*, 1981, vol. 119, p. 934.

17. Deirmendjian, D., *Electromagnetic Scattering on Spherical Polydispersions*, New York: American Elsevier, 1969, p. 290.

18. Wiscombe, W., Welch, R., and Hall, W., *J. Atmos. Sci.*, 1984, vol. 41, p. 1336.

19. Houze, R., Hobbs, P., Herzegh, P., et al., *J. Atmos. Sci.*, 1979, vol. 36, p. 156.

20. Schwartz, S.E, in *Chemistry of Multiphase Atmospheric Systems*, Jaeschke, W., Ed., Berlin: Springer, 1986, p. 415.

21. Langner, J. and Rodhe, H., *J. Atmos. Chem.*, 1951, vol. 13, p. 255.

22. Laj, P., Fuzzi, S., Facchini, M.C., et al., *Atmos. Environ.*, 1997, vol. 31, no. 16, p. 2503.

23. Laj, P., Fuzzi, S., Facchini, M.C., et al., *Atmos. Environ.*, 1997, vol. 31, no. 16, p. 2589.

24. Brock, J.R. and Durham, J.L., in *SO_2, NO, and NO_2 Oxidation Mechanisms: Atmospheric Considerations*, Calvert, J.G., Ed., Boston: Butterworth, 1984, p. 209.

25. Sedlak, D.L., Hoigne, J., David, M.M., et al., *Atmos. Environ.*, 1997, vol. 31, no. 16, p. 2515.